CFD SIMULATIONS OF BUOYANCY DRIVEN FLOW MIXING EXPERIMENTS PERFORMED AT THE ROCOM FACILITY

Log Number: 245

G. POCHET, Z. XINGYUAN and D. LEONARD

Tractebel Engineering, Brussels, Belgium guillaume.pochet@gdfsuez.com

Abstract

Multi-physics approaches are currently developed at Tractebel Engineering (TE) for accurately simulating the complex interaction between neutronics and thermal-hydraulics during asymmetric accidents. One branch of the improvements of the method focuses on the implementation in the coupled codes package of realistic core inlet distributions obtained from CFD results. Two flow mixing tests performed at the ROCOM facility and representative of asymmetric flow conditions are being simulated with the CFD code ANSYS CFX 12.0. The results show that the main mixing phenomena are qualitatively well reproduced, but a quantitative analysis points out an underestimation of the mixing in the simulations.

1. Introduction

In the framework of the accident analyses performed for the Final Safety Analysis Report, multiphysics approaches are developed at TE for asymmetric transients [1], with a strong emphasis on the Main Steam Line Break (MSLB) at Hot Zero Power (HZP) accident. During this accident, the excessive cooldown of the affected cold leg leads to a strong asymmetric temperature distribution at the core inlet. As a result, this excessive cooldown in one sector of the core might induce an increase of the reactivity and the reactor might return to power. The particular feature of this accident is that the neutronic response of the core is highly dependent on the temperature distribution at the core inlet. Thanks to the recent advances in computational resources and understanding of the physics, coupled neutronics and thermal-hydraulics codes have been developed at TE to accurately simulate this dependency. However, due to their 1D formulation and consequent limitations in modelling the flow mixing, the standard thermal-hydraulics system codes are unable to provide realistic core inlet distributions of the flow. More accurate modelling of the flow mixing can be obtained from CFD simulations. However, the integration of CFD core inlet flow distributions into the coupled calculations is a challenging task that requires the prior qualification of the CFD code. This qualification should be based on representative experiments regarding the applications foreseen. Therefore, two recent tests performed at the ROCOM facility in the framework of the OECD PKL2 project [2] represent an interesting benchmark, since the purpose of these tests is to investigate the flow mixing behaviour under asymmetric loop flow conditions. The first test simulates a MSLB transient and the second test simulates an Emergency Core Cooling (ECC) injection in two loops.

The structure of this paper is the following. In section 2 the ROCOM experimental facility is presented, and in section 3 the simulated experimental tests are described. The fourth section focuses on the CFD model and mesh generation methodology. In the fifth section the results of the CFD simulations are presented. The section first outlines the results of the sensitivity studies performed, which are of primary importance for determining the optimal mesh and simulation parameters to be used for the

final transient simulations. In the remaining of section 5, the calculations results are qualitatively and quantitatively compared to the experimental data. Finally, the main conclusions and future perspectives of the study are drawn in the last section.

2. The ROCOM experimental facility

ROCOM is an experimental facility located in Dresden-Rossendorf, Germany, and that was built to study the mixing phenomena in the vessel of pressurized water reactors. The facility is operated with water at room temperature and models a 4 loop KONVOÏ type reactor at the scale 1:5, including all geometrical features important for flow mixing. The scale mock-up is equipped with individually controllable pumps in order to allow simulating a large range of scenarios. Since water at room temperature is being used, temperature differences between the loops are simulated by density differences. This is carried out by adding a quantity of sugar to the water in order to adjust the relative densities between the loops. To quantify the flow mixing in the vessel, a quantity of salt is added to the water which acts as a tracer solution. The salted water can be traced through the vessel by recording electrical conductivity measurements. The measured electrical conductivity is proportional to the tracer concentration, and a mixing scalar is defined by the following expression:

$$\theta_{x,y,z}(t) = \frac{\sigma_{x,y,z}(t) - \sigma_0}{\sigma_1 - \sigma_0} \tag{1}$$

Log Number: 245

where σ_0 is the initial conductivity of the water in the vessel, σ_1 is the conductivity of the injected solution, and $\sigma_{x,y,z}(t)$ is the local conductivity measured. In order to ease the analysis of the experimental results and the comparison with CFD calculations, $\theta_{x,y,z}(t)$ is converted into a temperature value by the following expression:

$$T_{x,y,z}(t) = \theta_{x,y,z}(t) \times (T_1 - T_0) + T_0$$
(2)

where T₀ is the initial temperature of the water in the vessel and T₁ is the simulated temperature of the injected solution. For both experimental tests, three different types of wire-mesh sensors are used in the vessel to record electrical conductivity measurements with high resolution in space and time (up to 1000 Hz): two axial sensors in the downcomer (one in the internal cylindrical plane and one in the external cylindrical plane) with a resolution of 64 radial points x 29 axial points, one sensor with a resolution of 15 x 15 points at the core inlet, and three sensors with a resolution of 16 x 16 points in cold legs 3 and 4. Among the three cold leg sensors, one is located upstream of the ECC injection line and two are located downstream. An extensive validation work on the applicability of CFD methods for simulating previous ROCOM mixing experiments has already been performed and can be found in the literature ([3] to [7]).

3. Description of the simulated experiments

The two analysed tests simulate a MSLB and an ECC injection in two loops, respectively. The boundary conditions for both tests were derived from the experimental results of the PKL III G.3.1 test.

3.1 PKL III G.3.1 test

Figure 1 gives the time evolution of the average temperature in the 4 cold legs of the PKL facility during test G.3.1. This test simulates a MSLB test followed by an ECC injection in loops 1 and 4. At the beginning of the transient, the cold leg temperature of loop 1 continuously decreases and reaches a minimum temperature of 153° C at t = 609s, which is the selected state point for the boundary conditions of ROCOM Test 1.1. Starting from t = 1100s, the ECC injection is activated on loops 1 and 4, and ends up around t = 2200s. For ROCOM Test 1.2, the state point at t = 1500s is chosen as boundary conditions. The conversion of the PKL test results to boundary conditions for the ROCOM tests was performed by preserving the similarity of the Froude number, which gives the ratio between the inertia and gravitational forces:

$$Fr = \sqrt{\frac{\rho w^2}{\Delta \rho g L}} \tag{3}$$

To achieve the similarity of the Froude number, the original density difference in the PKL test was maintained and the velocity data were reduced by a factor of $\sqrt{5}$.

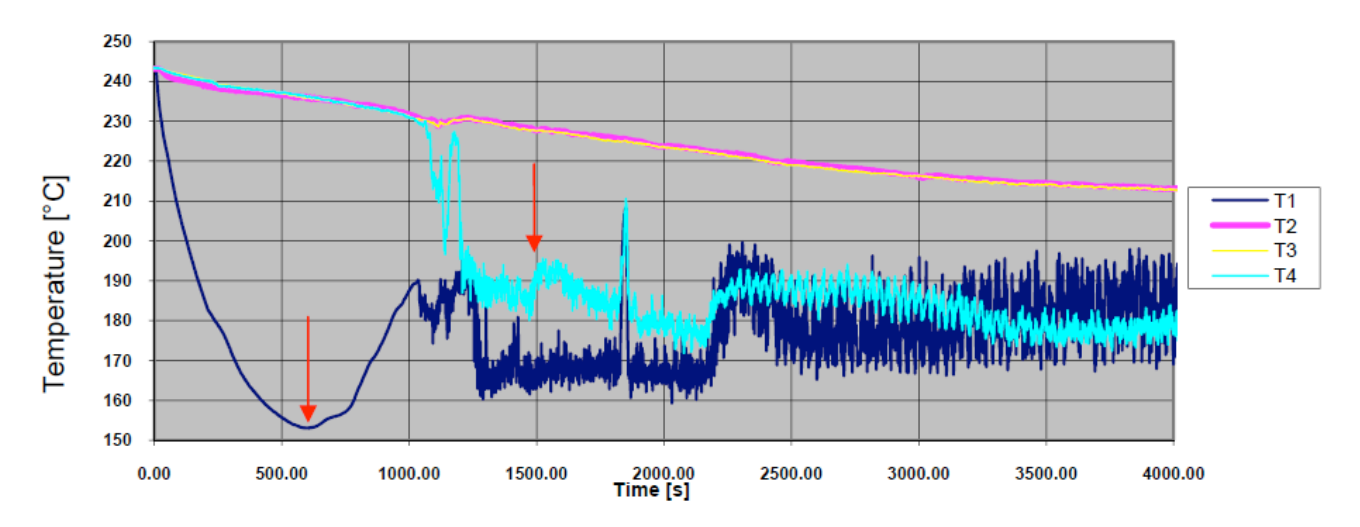


Figure 1 Time evolution of the cold legs average temperature during the PKL III G.3.1 test (red arrows indicate the selected state points for the boundary conditions of the two ROCOM tests)

3.2 ROCOM Test 1.1

The boundary conditions imposed during the first ROCOM test are summarized in Table 1. Prior the start of the experiment, a stable and identical mass flow is established in loops 2, 3 and 4, and the loop 1 flow is closed by switching off the valve located upstream of the water injection line. At t = 0s, the higher density water is injected in loop 1 with an important flow rate in order to simulate a MSLB transient, and the sensors start recording the data. The test lasts for 90 seconds in order to reach quasistationary flow conditions.

Table 1 Boundary conditions during ROCOM Test 1.1									
Loop	1 2 3 4								

Normalized volume flow rate [%]	12.21	3.15	3.15	3.15
Volume flow rate [m³/h]	22.6	5.8	5.8	5.8
Volume flow rate [l/s]	6.27	1.62	1.62	1.62
Relative density [-]	1.12	1.00	1.00	1.00

Log Number: 245

The boundary conditions given in the table above corresponds to the experimental conditions. In the CFD simulations, the mixing is simulated by temperature differences, in contrary to the experiment where the mixing is simulated by density differences. Therefore, in the CFD simulations of Test 1.1, a temperature of 153°C was imposed in cold leg 1, a temperature of 236.1°C was imposed in the remaining cold legs, and the flow rates given in Table 1 were considered. The same pressure as the one observed at the first state point of the PKL test was imposed (P = 3.8 MPa).

3.3 ROCOM Test 1.2

The boundary conditions imposed during the second ROCOM test are summarized in Table 2. Prior the start of the experiment, a stable and asymmetric flow rate is established in the loops, loop 3 simulating the affected loop in this case. At t = 0s, the ECC water is injected in loops 3 and 4 through their injection line and the sensors start recording the data. The test lasts for 110 s in order to reach quasistationary flow conditions.

Table 2 Boundary conditions during ROCOM Test 1.2

Loop	1	2	3	4	ECC
Normalized volume flow rate [%]	2.28	2.28	6.08	2.28	-
Volume flow rate [m³/h]	4.22	4.22	11.25	4.22	1.87
Volume flow rate [l/s]	1.17	1.17	3.12	1.17	0.52
Relative density [-]	1.00	1.00	1.00	1.00	1.2

The boundary conditions given in the table above corresponds to the experimental conditions. In the CFD simulations, the mixing is simulated by temperature differences, in contrary to the experiment where the mixing is simulated by density differences. Therefore, in the CFD simulations of Test 1.1, a temperature of 227.65°C was imposed in all cold legs, a temperature of 25°C was imposed in the ECC injection lines, and the flow rates given in Table 2 were considered. The same pressure as the one observed at the second state point of the PKL test was imposed (P = 3.97 MPa).

4. CFD model

4.1 Geometrical model

When modelling the pressure vessel, the geometrical details important for flow mixing have been resolved. In particular, the sieve drum located at the bottom of the vessel has been modelled in details. The real geometry of the core has been modelled, but a sensitivity study on the location of the outlet boundary condition has been performed (see Figure 2a and § 5.1). For the first test, the inlet of cold leg 1 can be modelled starting from the inlet nozzle or starting from the injection point of the water. Both models have been considered in the present study (see Figure 2a and § 5.1). For the second test, cold legs 3 and 4 have been extended and their ECC injection line has been modelled.

4.2 Mesh

Log Number: 245

Due to limited computational resources, mesh independent solutions could not be reached. Therefore, regions having the greatest mesh sensitivity have been refined to obtain the optimal mesh. The geometry has been divided in six regions (see Figure 2a), the mesh has been refined in all regions and the variation of the results has been analysed (see § 5.1). All the generated meshes are unstructured and hybrid. Hexahedral elements have been used where feasible (cold legs, downcomer and core), and for the remaining regions mostly tetrahedral elements have been used, but also pyramids and wedges. The different regions have been meshed together to achieve a proper connexion between the different element types. Layers of prismatic elements at the walls have been specified to capture the boundary layers effects. The height of the first layer adjacent to the walls was calculated to reach y⁺ values below 100. Figure 2b shows a visualization of the mesh in the different regions.

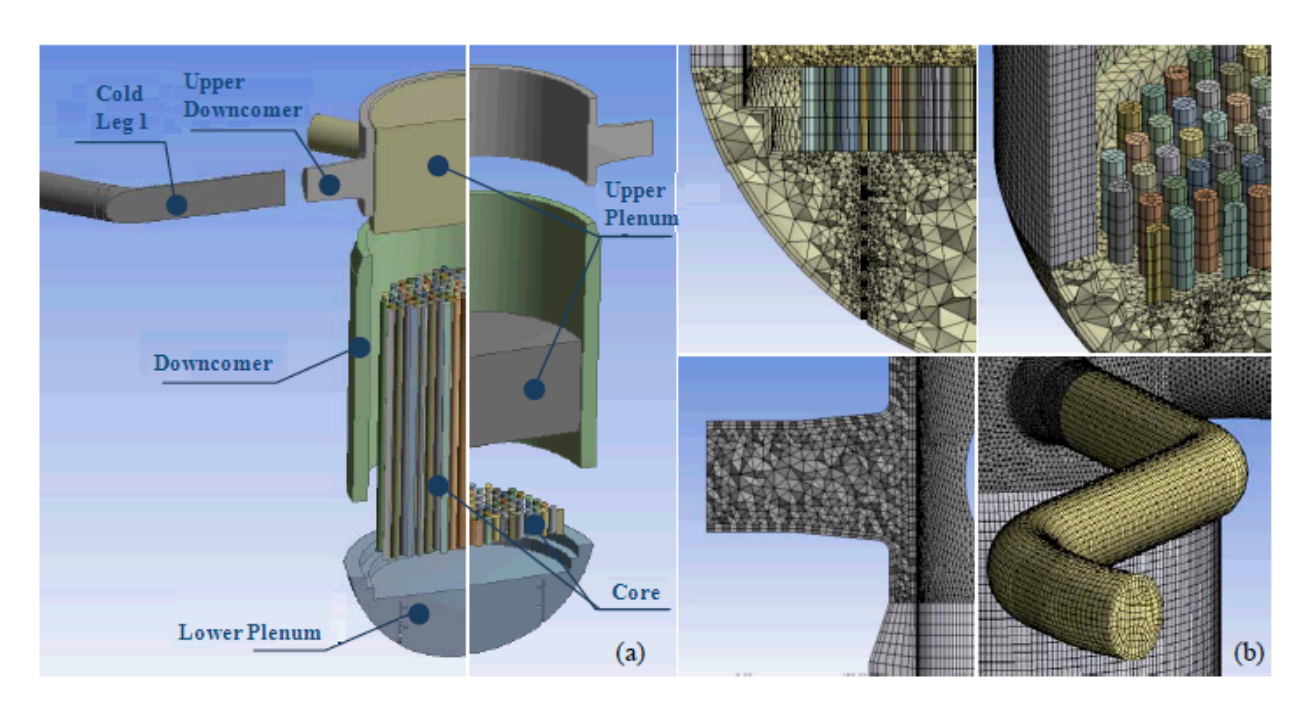


Figure 2 (a) different mesh regions; (b) visualization of the mesh

5. Simulations results

The aim of the present study is to analyse the flow mixing under quasi-stationary flow conditions. Therefore, time averaged experimental data have been provided [2]. Both steady-state (simulation of the final state of the experiments) and transient simulations (simulation of the whole experiments) have been performed. As they require less computational time, the steady-state simulations mostly aim at performing the sensitivity studies in order to determine optimal geometry, mesh and simulation models and methods.

5.1 Sensitivity studies

Because fluctuations of the flow field were observed in the steady-state simulations, each simulation was extended by 20s in transient mode with a time step of 0.05s. The results were time averaged over this 20s period and used as the basis for the sensitivity studies.

5.1.1 Geometry and mesh density

Table 3 presents the different meshes that have been generated for Test 1.1, depending on the mesh density of the different regions and the geometry. In the following analysis, Mesh 1 is considered as the reference mesh. For Test 1.1, two different geometry simplifications have been studied: the reduced core versus the full core, and the cold leg 1 inlet nozzle versus the extended cold leg 1.

Table 3 Mesh and geometrical sensitivity studies for Test 1.1

	Sensitivity	Upper						Total
Mesh	description	DC	DC	LP	UP	Core	Loops	elements
1	Reference	257 058	172 718	589 340	383 792	13 640	-	1 416 548
2	Full core, DC-	237 453	48 456	593 630	291 779	67 180	-	1 238 498
3	DC-	239 276	38 808	572 388	244 740	13 635	-	1 108 847
4	Upper DC+ and DC+	463 463	403 986	623 884	506 070	40 640	-	2 038 043
5	LP+	256 813	172 718	970 017	403 675	20 355	-	1 823 578
6	LP++	261 438	197 136	1 466 056	474 956	24 375	-	2 423 961
7	Core+	256 899	174 397	1 162 280	842 980	197 750	-	2 634 306
8	Extended cold leg 1	257 845	166 392	673 392	474 663	16 170	35 328	1 623 790

^{- :} reduced density

To determine the optimal mesh and geometry, a Root Mean Square (RMS) temperature error was calculated at each sensor, taking into account all measurement points. The calculated RMS error is defined by the following expression:

$$Error_{RMS} = \sqrt{\frac{1}{n} \sum_{i=1}^{n} Error_{i}^{2}}$$
 (4)

Log Number: 245

$$Error_{i} = \frac{Measured_{i} - Calculated_{i}}{Measured_{i}} \times 100$$
(5)

where Error_i is equal to the relative error in % units between the measured and calculated value in °C units at point i and n is the number of measurement points. Table 4 gives the calculated RMS temperature errors at the different sensors for Test 1.1 for each mesh generated. From this table it can be observed that the geometry simplification on the core has a significant impact. Indeed, the RMS temperature error at the core sensor is significantly decreased when taking into account the real geometry of the core. This might be due to the fact that in the present test the flow is density driven, and the buoyancy forces have a great influence on the flow field. When looking at the RMS errors for meshes 1 to 3, it is concluded that the geometry simplification on the core only impacts the solution at the core sensor. Indeed, the different RMS errors at the downcomer sensors for Mesh 2 are due to the mesh density variation in the downcomer. In addition, it can be observed that the RMS error at the core sensor is only slightly affected by the mesh density variation in the downcomer (see RMS temperature error at the core sensor for mesh 3). The RMS errors for meshes 5 and 6 also lead to the conclusion that the influence on the solution of the mesh density variation in the lower plenum is weak. The impact of the mesh density variation in the core is a bit higher (see RMS temperature errors for mesh 7). The geometry simplification on the cold leg of loop 1 also gives a significant impact on the solution, especially at the downcomer sensors (see RMS temperature errors for mesh 8). This is probably due to the fact that modelling the cold leg from the injection point allows for the flow to develop before

^{+:} increased density

entering the pressure vessel. In general, the RMS errors are the greatest at the downcomer sensors for Tests 1.1. This results from the disagreements observed in the region below the inlet nozzle of the affected cold leg 1, and in the stratification region (see § 5.2.1).

Log Number: 245

Following these sensitivity studies, it is recommended to model the real geometry of the core and the cold leg 1 starting from the injection point. In addition, the mesh density should be increased in the downcomer and core region, as well as in the lower plenum but to a lower extent. Table 5 gives the characteristics of the optimal mesh that was generated for Test 1.1. Table 4 shows that the sum of the three RMS errors is the smallest for the final mesh, which confirms the conclusions of the geometry and mesh sensitivity studies.

Table 4 RMS temperature errors at the different sensors for Test 1.1

Tuble 114,15 temperature errors at the different sensors for rest in							
Mesh	h RMS error RMS error core sensor [%] inner DC sensor [RMS error outer DC sensor [%]				
1	2.1	8.7	8.7				
2	1.4	7.6	7.6				
3	2.0	7.7	7.7				
4	2.0	8.4	8.3				
5	2.0	8.7	8.8				
6	2.0	8.4	8.5				
7	1.9	8.7	8.2				
8	1.9	8.0	8.1				
Final	1.4	7.2	7.7				

Table 5 Final mesh for Test 1.1

Mesh	Geometry description	Upper DC	DC	LP	UP	Core	Loop 1	Total elements
Final	Full core, extended	1 053 468	627 186	1 497 182	392 023	326 500	62 403	3 958 942
	cold leg 1							

5.1.2 Turbulence model

Based on the final mesh presented in Table 5, two calculations with different turbulence models have been performed: one calculation with the SST (Shear Stress Transport) k- ω turbulence model, and one with the standard k- ϵ model. The choice of one or the other model has been found to have a significant impact on the flow field in the downcomer, and to a lower extent on the flow field at the core inlet. Figure 3 giving the velocity streamlines in the vessel for both models shows that angular spreading of the flow at the inlet nozzle is smaller when using the k- ϵ model. When comparing the RMS errors for both calculations, it has been observed that the error at the downcomer sensors is reduced by 1.5 % (at the inner plane) and by 2 % (at the outer plane) when using the k- ϵ model. However, the error at the core sensor is increased by 0.2 % when using the k- ϵ model features a more accurate treatment near the wall by automatically switching from wall functions to a low Reynolds number formulation. Therefore, it was decided to perform the final transient simulations with the SST k- ω turbulence model. The use of a second order turbulence model such as the Reynolds Stress model would be recommended for the studied cases but has not been considered due to the increased computational time needed for performing the simulations with such a model.

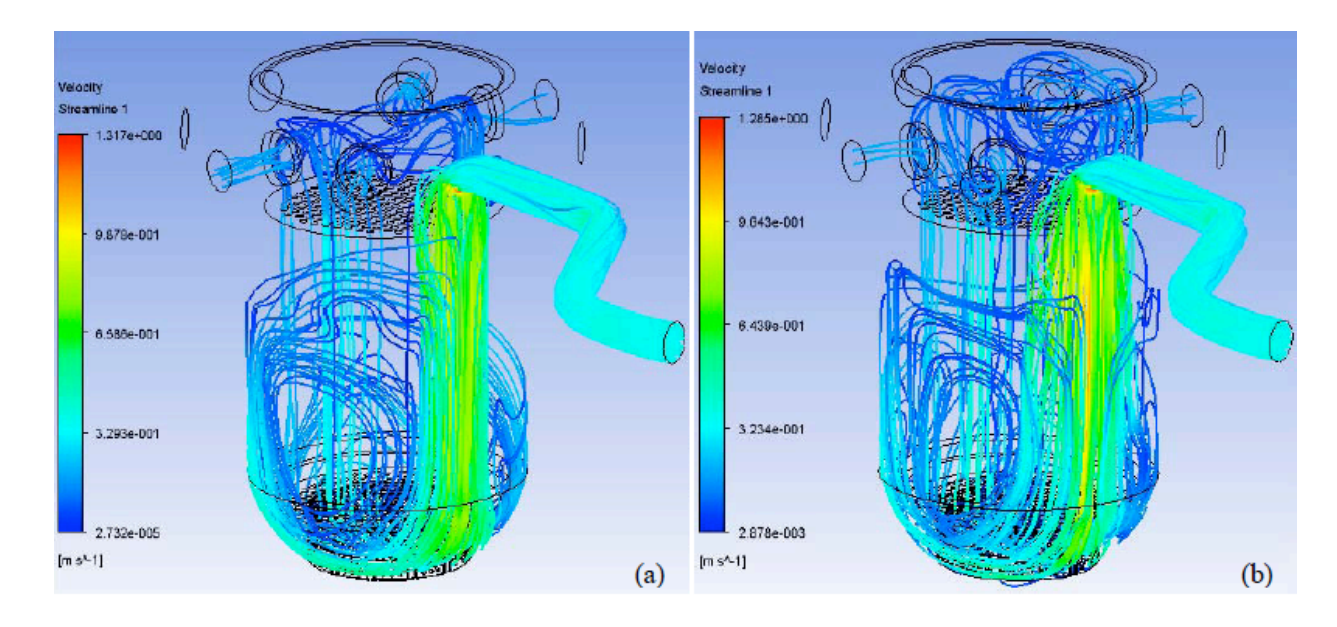


Figure 3 Velocity streamlines in the vessel: (a) k-ε model; (b) k-ω SST model

5.2 Transient simulations

Following the conclusions of the sensitivity studies, the optimal mesh and simulation parameters have been considered for running full transient simulations of the experiments. More precisely, the SST k- ω turbulence model and the second order high resolution numerical scheme of ANSYS CFX for the spatial discretization have been chosen. For the time discretization, the second order backward Euler scheme has been specified. For the physical properties, the standard IAPXS IS97 water tables have been used. For each simulation, the transient results were time averaged in order to make a relevant comparison to the experimental data.

5.2.1 <u>Test 1.1</u>

Figure 4 gives the time averaged temperature profile at the core and downcomer sensors for both the CFD results and the experimental data. For the transient simulation, an adaptative timestep with minimum value 0.01s and maximum value 1s has been chosen. From Figure 4 it can be observed that the calculation results show qualitatively a good agreement with the experimental data, since, all the relevant mixing phenomena observed in the experiment are reproduced in the simulation. In both cases, a stratification establishes along the height of the downcomer, in the inner as well as in the outer plane, which means that there is already an important mixing of the flow in the downcomer. The calculated minimum temperature at the core inlet sensor is really close to the experimental data (181°C – 182°C) and is observed near the same location, that is, at the azimuthal position below the inlet nozzle of loop 1. In both the simulation and the experiment, the greatest temperatures at the core inlet are found at the periphery, outside of the sieve drum. When comparing steady-state and transient simulations results for this test, it has been observed that the minimum, maximum and average temperature values at the core sensor are different. The calculated maximum and average values are lower in the steady-state simulation (193°C and 184°C), and the calculated minimum is higher (182°C). This is due to the fact that the steady-state simulation calculates a final state, whereas the transient simulation is not fully stable yet during the averaging time interval, and the core inlet temperature continues to decrease. When looking at the RMS error at the core sensor for both calculations (see Table 6), it is found that

the error is 1.1% lower in the steady-state simulation. Therefore, for Test 1.1 it is concluded thata steady-state simulation may be used instead of a transient simulation.

When compared to the simulation, the stratification in the experiment establishes at a lower position in the downcomer. However, the calculated average temperature in the inner downcomer plane is in close agreement with the experimental data $(201^{\circ}\text{C} - 202^{\circ}\text{C})$. Regarding the azimuthal temperature profile in the downcomer, there is a disagreement between calculation and experiment at both sensors. Indeed, in the simulation the spreading of the cold water below the inlet nozzle is underestimated in the outer plane (top figure) and overestimated in the inner plane (bottom figure). In addition, the mixing along the flowpath is underestimated in the calculation, since it can be seen at the inner downcomer plane that the stream of cold propagates along the full height in the calculation.

At the core inlet sensor, there is a disagreement between calculation and experimental data for the maximum temperature, since the calculated maximum temperature is 10°C higher. This confirms the fact that the mixing is underestimated in the simulation. This effect also results from the insufficient mixing of the cold water in the downcomer

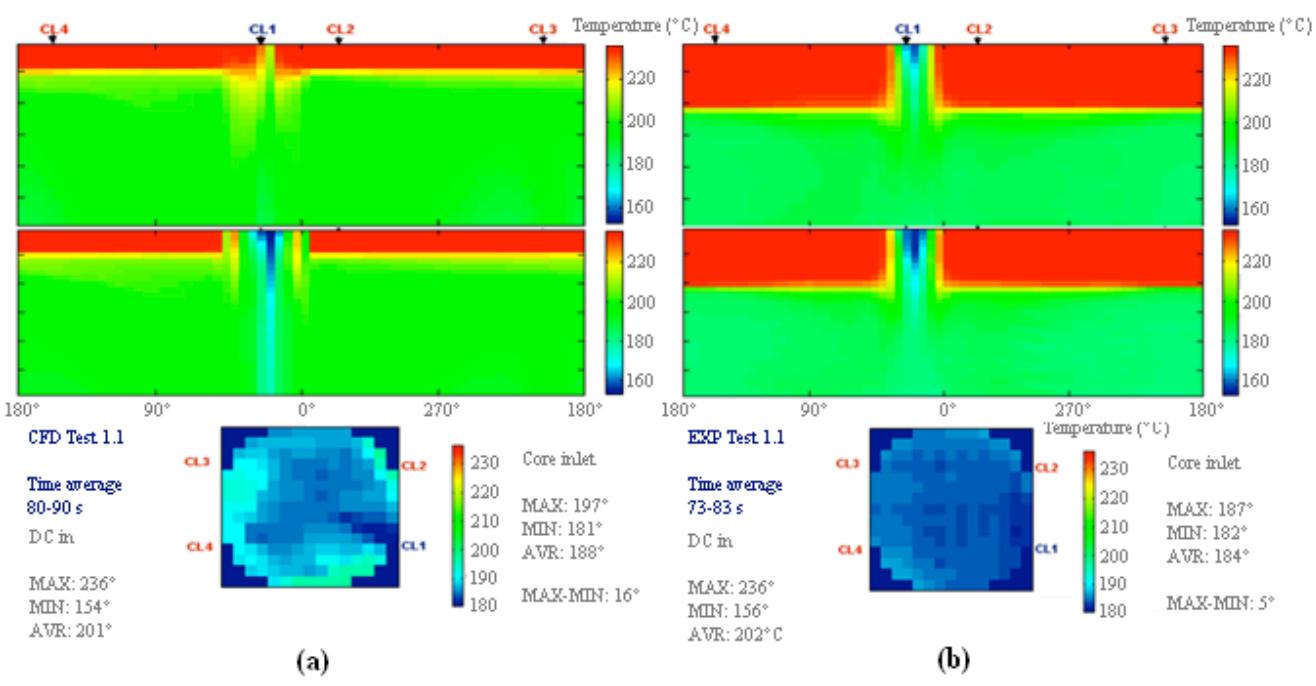


Figure 4 Time averaged temperature profile at the core and downcomer sensors for Test 1.1: (a) CFD results; (b) experimental data

Table 6 RMS temperature errors at the different sensors for the simulations of Test 1.1

Simulation	RMS error core sensor [%]	RMS error inner DC sensor [%]	RMS error outer DC sensor [%]
Transient	2.5	7.2	7.5
Steady-state	1.4	7.2	7.7

5.2.2 Test 1.2

Figure 5 gives the averaged temperature profile at the core, downcomer and loops sensors for both the CFD results and the experimental data. Both the experimental and calculation results have been time averaged over the same time interval (40-50s for the loops sensors, 60-70s for the downcomer and core sensors). For the transient simulation, an adaptative timestep with minimum value 0.001s and maximum value 1s has been chosen. From the figure it can be observed that both in the calculation and in the experiment, the temperature profile in both planes of the downcomer is similar. However, the mixing of the cold ECC water in the downcomer is more intensive in the experiment. Indeed, in the experiment the streams of the cold ECC water disappear around the mid-height of the downcomer, whereas in the calculation the cold streams are observed along the full height in the outer plane.

Log Number: 245

At the core inlet, both the simulation and the experiment show a nearly uniform temperature profile, with only 2°C difference between the minimum and maximum values. However, there is a shift of the average temperature of +13°C between the experiment and the calculation. It has been observed in the time evolution of the temperatures (which are not presented here) that the decrease of the average temperature at the core inlet sensor is well faster in the calculation than in the experiment, which also points out the underestimated mixing in the calculation. There is also a disagreement when comparing both core inlet temperature profiles, where in the experiment the lowest temperatures are observed below the inlet nozzle of loop 4, whereas in the calculation they are found near the centre of the core. When comparing the results of the steady-state simulation (which are not presented here) to the experiment, it was found that the temperature shift of the average temperature is even higher (+18°C). This is due to the fact that the steady-state calculation computes a final state, whereas in the experiment, after 70s the temperature field at the core inlet is not stable yet and continues to decrease. Therefore, for this test it is concluded that a transient simulation provides better results (see calculated RMS errors in Table 7).

When looking at the results at the loops sensors, it is found that the calculated temperature profile is in good agreement with the experimental data for the sensors of loop 3. However, for the sensor located upstream of the ECC injection line in loop 3 (sensor L31), the calculation predicts a slight ECC reverse flow that is not observed in the experiment. For the sensors of loop 4 where the flow rate is smaller, there is a disagreement between calculation and experiment. In the calculation, the stratification between the cold and hot water is more spread than in the experiment. As a result, the minimum temperature is well lower in the experiment. This is the inverse situation as observed for the downcomer and core sensors: the CFD simulation overestimates the flow mixing in the loops. This disagreement between simulation results and experimental data at the loops sensors is thought to be due to the inlet boundary conditions considered for the ECC injection lines. Since no data are available for the velocity profile at the ECC injections, a uniform velocity profile was imposed in the simulation. However, the velocity profile in the ECC injection line is expected to have a significant impact on the flow mixing in the loops.

Table 7 RMS temperature errors at the different sensors for the simulations of Test 1.2

Simulation	RMS core sensor [%]	RMS inner DC sensor [%]	RMS outer DC sensor [%]	RMS loop 3 sensors [%]	RMS loop 4 sensors [%]
Transient	5.4	3.2	3.1	41.2/53.9	50.1/47.4/60.7
Steady-state	8.2	8.5	8.4	41.2/53.9	48.3/46.5/60.3

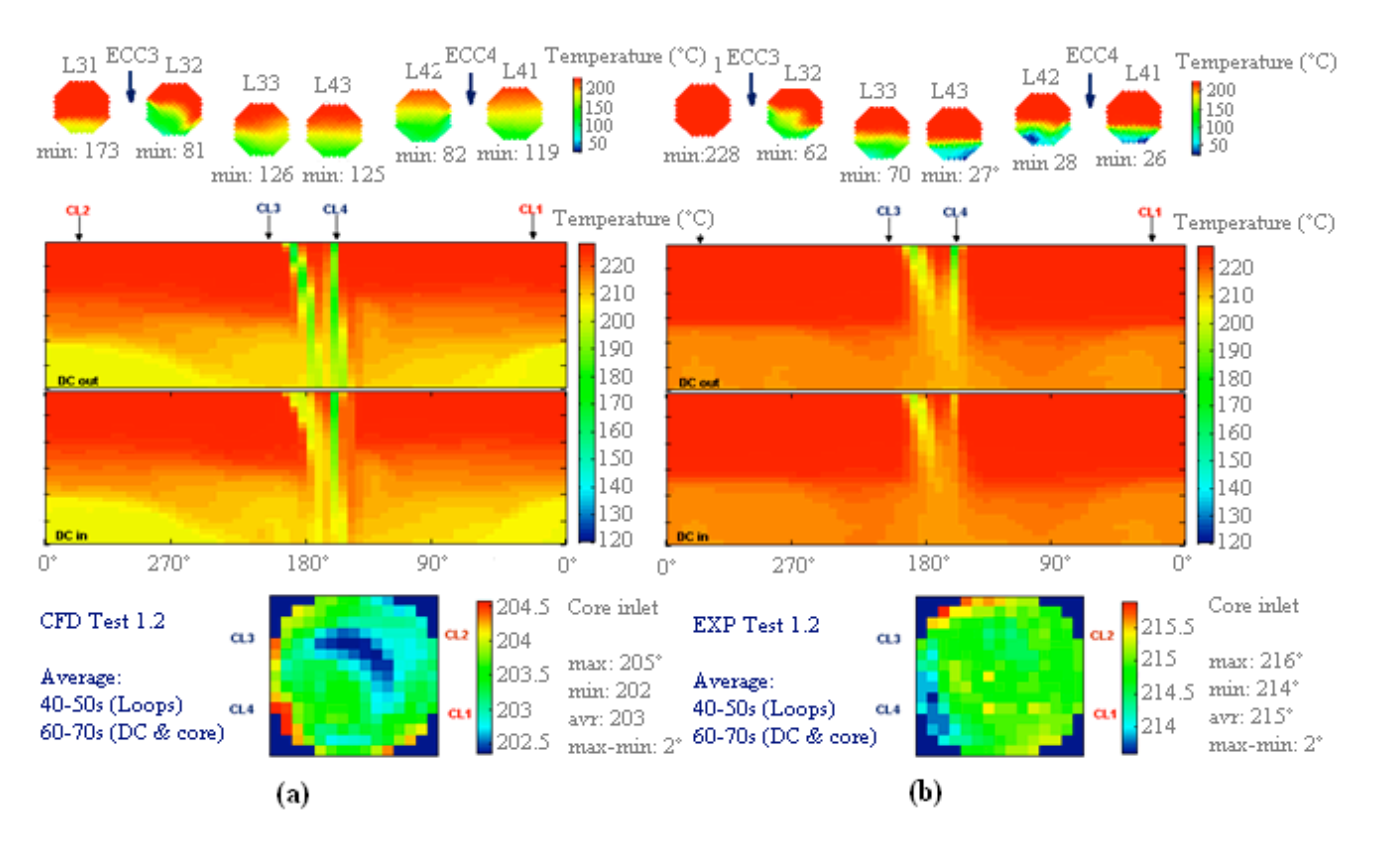


Figure 5 Time averaged temperature profile at the core, downcomer and loops sensors for Test 1.2: (a) CFD results; (b) experimental data

6. Conclusion

In the present study, CFD simulations of two recent flow mixing tests performed at the ROCOM facility have been performed. These tests have the particularity that they focus on representative situations arising during asymmetric transients. Therefore, as the principal goal of the work is to qualify the CFD code for flow mixing analysis in pressure vessels during asymmetric accidents, the proper simulation of these tests is of primary importance. The simulated tests also have the important characteristic that they are at low flow rate, and therefore buoyancy dominated.

Sensitivity studies have been carried out, taking into account the impact of geometry simplifications, mesh density and turbulence models. These sensitivity studies have shown the importance of the simulations parameters on the results and provide guidelines for modelling similar experiments with CFD. Steady-state as well as transient simulations have been performed. In the present tests, the results of both types of simulations show differences because an equilibrium state is not fully reached in the experiments, and particularly for the ECC injection test. The work has shown that the buoyancy driven experiments can be qualitatively well reproduced by the CFD code, since the main mixing phenomena can be predicted: quasi-uniformity of the temperature profile at the core inlet, stratification region in the downcomer and reverse ECC flow. However, a quantitative analysis shows that there exists significant disagreements between the CFD solutions and the experimental data. Indeed, for both tests the CFD code underestimates the mixing in the vessel. However, at the loops sensors the inverse effect is observed, where the CFD code overestimates the mixing.

Further investigations should be carried out on the CFD simulations. In particular, the mesh sensitivity study should be extended, which was not feasible in the present case because of limited computational resources. In addition, more precise details of the inlet boundary conditions at the ECC injection lines should be provided for Test 1.2 in order to explain the disagreement observed at the loops sensors. The disagreement between calculations and experiments might also come from the fact that the nature of the flow is different between both cases. In the experiment, the mixing is simulated by adding sugar to the water in order to manipulate the density of the water. However, in the CFD simulations, the mixing is simulated by temperature differences. The similarity between tracer concentration and coolant temperature might be assumed in the case where the turbulent mixing is dominating. This assumption should therefore be verified in cases of low flow rates as those encountered in the simulated tests.

Log Number: 245

7. References

- [1] G. Pochet, M. Haedens, C.R. Schneidesch, D. Léonard, "CFD simulations of the flow mixing in the lower plenum of PWR's", <u>CFD4NRS-3: Experimental Validation and Application of CFD and CMFD</u> Codes to Nuclear Reactor Safety Issues, Washington D.C., USA, 14-16 September 2010
- [2] S. Kliem, R. Franz, "Quick-look report of the ROCOM Tests 1.1 and 1.2 conducted within the OECD PKL2 Project", Report FZD\FWS\2010\07, 2010
- [3] T. Höhne, S. Kliem, "Modeling of a Buoyancy-Driven Flow experiment in Pressurized Water Reactors using CFD-Methods", *Nuclear Engineering and Technology*, Vol. 39, Iss. 4, 2007, pp.327-336
- [4] T. Höhne, "Numerical simulation of coolant mixing in a pressurized water reactor with different CFD methods based on complex meshes", *International Journal of Nuclear Energy Science and Technology*, Vol. 3, Iss. 4, pp.399-412
- [5] S. Kliem, T. Höhne, U. Rohde, F.-P. Weiss, "Experiments on slug mixing under natural circulation conditions at the ROCOM test facility using high-resolution measurement techniques and numerical modeling", *Nuclear Engineering and Design*, Vol. 240, Iss. 9, 2010, pp.2271-2280
- [6] H.-M. Prasser, G. Grunwald, T. Höhne, S. Kliem, U. Rohde, F.-P. Weiss, "Coolant mixing in a PWR deboration transients, steam line breaks and emergency core cooling injection experiments and analyses", *Nuclear Technology*, Vol. 143, Iss. 1, 2003, pp.37-56
- [7] U. Rohde et al., "Fluid mixing and flow distribution in a primary circuit of a nuclear pressurized water reactor Validation of CFD codes", *Nuclear Engineering and Design*, Vol. 237, Iss. 15-17, 2007, pp.1639–1655